TECHNICAL RESEARCH REPORT

Analysis of a high-resolution optical wave-front control system

by E.W. Justh, P.S. Krishnaprasad

CDCSS TR 2002-2
(ISR TR 2002-5)

The Center for Dynamics and Control of Smart Structures (CDCSS) is a joint Harvard University, Boston University, University of Maryland center, supported by the Army Research Office under the ODDR&E MURI97 Program Grant No. DAAG55-97-1-0114 (through Harvard University). This document is a technical report in the CDCSS series originating at the University of Maryland.

Web site http://www.isr.umd.edu/CDCSS/cdcss.html

Analysis of a high-resolution optical wave-front control system

E. W. Justh and P. S. Krishnaprasad[1]
Institute for Systems Research and
Department of Electrical and Computer Engineering
University of Maryland
College Park, MD 20742, USA
e-mail: justh@isr.umd.edu, krishna@isr.umd.edu

Abstract — **We consider the formulation and analysis of a problem of automatic control: correcting for the distortion induced in an optical wave front due to propagation through a turbulent atmosphere. It has recently been demonstrated that high-resolution optical wave-front distortion suppression can be achieved using feedback systems based on high-resolution spatial light modulators and phase-contrast techniques. We examine the modeling and analysis of such systems, for the purpose of refining their design. The approach taken here might also be applicable to other problems involving feedback control of physical fields, particularly if the field sensing is performed optically.**

I. Introduction

Correcting for the distortion induced in an optical wave front due to propagation through a turbulent atmosphere can be formulated as problem of automatic control. Thermal gradients in the air produce index-of-refraction variations experienced by light which passes through it, leading to wave-front distortion. Wave-front correction is achieved by applying (e.g., using an array of micromirrors) conjugate distortions to produce net null distortion. *Adaptive optics* is the discipline concerned with feedback compensation of wave-front distortion in real-time.

A key criterion for an adaptive optic system is the resolution required for wave-front control (or conjugation), which in turn depends on the optical wavelength and on the strength of the turbulence. Stronger turbulence also requires an adaptive optic system to have a faster response (i.e., a higher frame rate). Recent advances in high-resolution liquid-crystal (LC) and microelectromechanical (MEMS) devices have led to spatial light modulators (SLMs) that meet both the speed and resolution requirements for high-resolution ($> 10^4$ actuators) adaptive optics [1, 2]. However, in addition to the devices, there is also a need for control laws which scale appropriately in this high-resolution, high-speed regime. Suitable control laws based on high-resolution SLMs and phase-contrast techniques have recently been demonstrated [3, 4]. Our focus here is on the modeling and analysis of these systems, extending earlier work [5].

In the next section we briefly review the high-resolution wave-front control system architecture and its origins. In Section III, we introduce the mathematical models and analyze them. In Section IV, we digress from the analysis to clarify certain practical issues and provide context for the mathematical work. In Section V, we consider the wave-front control system as a wave-front estimator. Concluding remarks appear in Section VI.

[1]This research was supported in part by grants from the Army Research Office under the ODDR&E MURI97 Program Grant No. DAAG55-97-1-0114 to the Center for Dynamics and Control of Smart Structures (through Harvard University), and by the National Science Foundation under the Learning and Intelligent Systems Initiative Grant CMS 9720334.

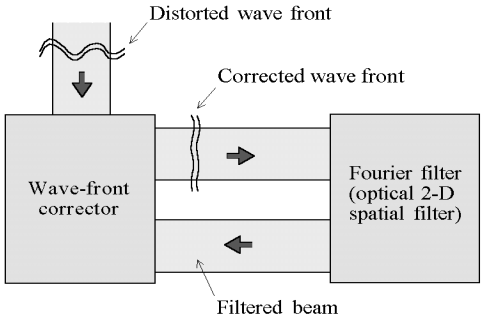

Fig. 1: High-resolution wave-front control system block diagram.

II. High-resolution wave-front control system

The general system architecture we consider is shown in figure 1. The distorted beam enters the wave-front corrector, which modulates the wave front with the objective of canceling the distortion. The corrected beam is then filtered using a controlled optical two-dimensional spatial Fourier filter, and the resulting filtered beam is used to update the wave-front corrector. The control system design problem involves choosing the wave-front corrector update law and the Fourier filter so as to ensure stability, and convergence to a wave-front-distortion-free corrected beam in as few iterations as possible.

Both the wave-front corrector and the controlled Fourier filter use a high-resolution SLM and a high-resolution imager, as shown in figures 2 and 3. The key feature of the system of figure 1 is that the subblocks shown in figures 2 and 3 can use parallel, distributed processing between the imagers and SLMs. That is, each SLM pixel is driven by the corresponding camera pixel (with any additional controls being common to all pixels). This feature, refered to in adaptive optics as "direct control," enables the resolution to scale without impacting system speed.

The system of figure 1 has its roots in the phase-contrast technique developed by Frits Zernike during the 1930s (for which he was later awarded a Nobel Prize in physics) [6]. Zernike observed that the system of figure 3 (without the imager and with the SLM replaced by a fixed phase plate having a centered phase-shifting dot to shift only the zero-order Fourier component) is capable of producing an intensity image related to the input beam wave front [7]. Zernike's technique has found application in phase-contrast microscopes for many

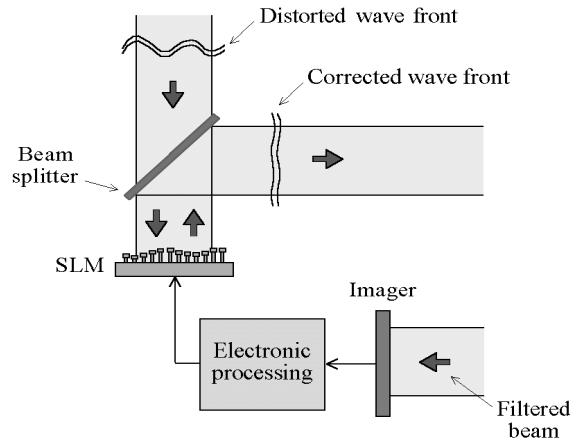

Fig. 2: Opto-electronically controlled wave-front corrector.

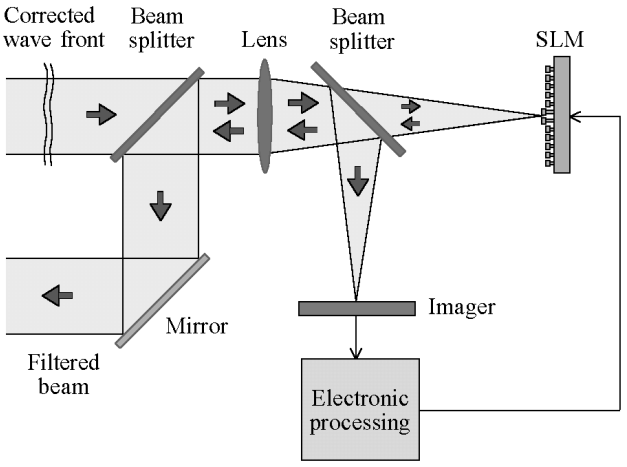

Fig. 3: Opto-electronically controlled spatial Fourier filter.

years [8]. Recent advances in high-resolution SLMs have led to renewed interest in phase-contrast techinques for various applications, including adaptive optics [3, 4, 9, 10].

The system of figure 1 is a nonlinear feedback system, because the wave-front phase of the corrected beam enters nonlinearly into the filtered beam intensity image. The Fourier filter operator, i.e., the mapping from the Fourier-domain imager to the Fourier filter, introduces further nonlinearity, and this additional source of nonlinearity turns out to be essential to producing a practical wave-front control system. Addressing these nonlinear effects is the main contribution of the analysis presented here and in [5].

III. Mathematical models

The key to successful analysis of this type of system is to capture the underlying physics with sufficient fidelity, while keeping the nonlinear modeling simple enough to extract qualitative insights beyond what a linearized approximation to the dynamics can provide. To describe the optical field (for a monochromatic beam), we introduce a complex envelope $A(x, y, z)$, describing a single component of the electric or magnetic field. We distinguish the z direction as the "optical axis," and denote the transverse coordinates as $\mathbf{r} = (x, y)$. The underlying electromagnetic field component that $A(\mathbf{r}, z)$ represents is then obtained by taking the real part of $A(\mathbf{r}, z)\mathrm{e}^{i(\omega t - kz)}$, where $k = 2\pi/\lambda$ and $\omega = kc$ (with λ the optical wavelength, and c the speed of light).

The complex envelope $A(\mathbf{r}, z)$ can be expressed in polar form as

$$A(\mathbf{r}, z) = a(\mathbf{r}, z)\mathrm{e}^{i\phi(\mathbf{r},z)}, \tag{1}$$

where $[a(\mathbf{r}, z)]^2$ is the intensity and $\phi(\mathbf{r}, z)$ is the phase (the quantity we are interested in measuring and controlling). The intensity is what a camera would measure at the point z along the optical axis.

In the wave-front control setting, we are interested in how the phase at a particular point z_0 along the optical axis evolves in time. Therefore, we drop the argument z from equation (1), and we allow ϕ to depend on a time variable t. (This time variable corresponds to quasi-static changes in the complex envelope, not the time scale of electromagnetic field oscillations.) Because we assume that $a(\mathbf{r}) = 0$ outside of a bounded region, we can use a Fourier series representation:

$$\begin{aligned} A(\mathbf{r}, t) &= \sum_{\mathbf{p}} \mathrm{a}_{\mathbf{p}}(t)\mathrm{e}^{i\frac{2\pi}{\gamma}\mathbf{p}\cdot\mathbf{r}}, \\ \mathrm{a}_{\mathbf{p}}(t) &= \frac{1}{\gamma^2}\int A(\mathbf{r}, t)\mathrm{e}^{-i\frac{2\pi}{\gamma}\mathbf{p}\cdot\mathbf{r}}d\mathbf{r}, \end{aligned} \tag{2}$$

where $\mathbf{p}$ is an ordered pair of integers (i.e., $\mathbf{p}$ takes values in the integer lattice in the plane), and γ is a beam-size parameter determining the spectral resolution (assumed sufficiently fine to avoid aliasing). Without loss of generality, we assume $a(\mathbf{r}) = 0$ outside of a square region Ω with sides of length γ. The integral in equation (2) can then be considered an integral over Ω, and $A(\mathbf{r}, t)$ can be intepreted as a spatially periodic function satisfying

$$A(x + m_x\gamma, y + m_y\gamma, t) = A(x, y, t), \tag{3}$$

where m_x and m_y are arbitrary integers. This interpretation of the Fourier series representation gives rise to periodic boundary conditions for the PDE systems introduced below.

A. *Single-pixel Fourier phase filter*

Suppose only the zero-order Fourier component is phase-shifted by the SLM in figure 3. Let the distorted beam complex envelope in figure 1 be represented as $a(\mathbf{r})\mathrm{e}^{i\phi(\mathbf{r})}$, and let the wave-front-correcting SLM impose a phase distribution $u(\mathbf{r}, t)$ on the distorted beam. The corrected beam is then represented by $a(\mathbf{r})\mathrm{e}^{i[u(\mathbf{r},t)+\phi(\mathbf{r})]}$. We denote the filtered image by $[f(u + \phi)](\mathbf{r}, t)$ to emphasize that it is a functional of the phase of the corrected wave front. The evolution equation we assume for u is

$$\frac{\partial u}{\partial t} = \eta\left[l^2\Delta u - f(u + \phi)\right], \tag{4}$$

where the gain function η satifies $\eta(\mathbf{r}, t) > 0$, $\forall \mathbf{r}, t$. The diffusion term can be considered strictly as an aid to analysis, with the diffusion length $l > 0$ being arbitrary small.

The dynamics are thus determined by f, which captures the effects of the Fourier phase filtering of the corrected beam. Besides the phase-shift of the zero-order Fourier component, there is also an intensity measurement included in f. Letting θ represent the phase-shift of the zero-order Fourier component, we thus obtain the following conventional Zernike wave-front sensor model:

$$\begin{aligned} &[f_{conv}(u + \phi)](\mathbf{r}, t) \\ &= \left|a(\mathbf{r})\mathrm{e}^{i[u(\mathbf{r},t)+\phi(\mathbf{r})]} + (\mathrm{e}^{i\theta}{-}1)\frac{1}{\gamma^2}\int a(\mathbf{r})\mathrm{e}^{i[u(\mathbf{r},t)+\phi(\mathbf{r})]}d\mathbf{r}\right|^2. \end{aligned} \tag{5}$$

(We have ignored finite aperature effects by failing to truncate the Fourier series at some finite frequency.)

Some of the undesirable nonlinearities present in f_{conv} can be cancelled by taking the difference of two such images, corresponding to oppositely-directed Fourier phase-shifts [3, 4, 5] (a related idea can be found in [11]). The resulting "differential" Zernike wave-front sensor model is

$$\begin{aligned}
&[f_{diff}(u+\phi)](\mathbf{r},t)\\
&= \left| a(\mathbf{r})\mathrm{e}^{i[u(\mathbf{r},t)+\phi(\mathbf{r})]} + (\mathrm{e}^{i\theta}-1)\frac{1}{\gamma^2}\int a(\mathbf{r})\mathrm{e}^{i[u(\mathbf{r},t)+\phi(\mathbf{r})]}d\mathbf{r}\right|^2\\
&- \left| a(\mathbf{r})\mathrm{e}^{i[u(\mathbf{r},t)+\phi(\mathbf{r})]} + (\mathrm{e}^{-i\theta}-1)\frac{1}{\gamma^2}\int a(\mathbf{r})\mathrm{e}^{i[u(\mathbf{r},t)+\phi(\mathbf{r})]}d\mathbf{r}\right|^2\\
&= -4\sin\theta\ \mathrm{Im}\left\{a(\mathbf{r})\mathrm{e}^{-i[u(\mathbf{r},t)+\phi(\mathbf{r})]}\frac{1}{\gamma^2}\int a(\mathbf{r})\mathrm{e}^{i[u(\mathbf{r},t)+\phi(\mathbf{r})]}d\mathbf{r}\right\}. \quad (6)
\end{aligned}$$

The image subtraction required for the differential wave-front sensor can potentially be incorporated into the circuitry of the imager in figure 2 [12]. The differential Zernike wave-front sensor image given by equation (6) is straightforward to interpret. At each point $\mathbf{r}$ (and for fixed t), the value of the operator f_{diff} is a periodic function of the corrected beam phase. However, there is also global coupling through the zero-order Fourier component $\frac{1}{\gamma^2}\int a(\mathbf{r})\mathrm{e}^{i[u(\mathbf{r},t)+\phi(\mathbf{r})]}d\mathbf{r}$.

The dynamics given by equation (4), with $l = 0$ and f given by equation (6), are (formally) gradient dynamics with respect to the energy functional

$$[V(u)](t) = -2\gamma^2\sin\theta\left|\frac{1}{\gamma^2}\int a(\mathbf{r})\mathrm{e}^{i[u(\mathbf{r},t)+\phi(\mathbf{r})]}d\mathbf{r}\right|^2, \quad (7)$$

which is proportional to (the negative of) the intensity in the zero-order Fourier component of the corrected beam [4, 5].

Remark on notation: We will generally drop the $\mathbf{r}$ and t arguments of u and $f(u+\phi)$, as well as the $\mathbf{r}$ argument of a and ϕ, in the remainder of the development. The equations are then more compact and easy to read, but a, ϕ, and u must be interpreted as functions, and f as an operator.

Using variational calculus, for equation (4) with $l = 0$, we obtain

$$\begin{aligned}
\frac{dV}{dt} &= \frac{\delta V}{\delta u}\cdot\frac{\partial u}{\partial t}\\
&= -4\sin\theta\ \mathrm{Re}\left\{\int a(\mathbf{r})\mathrm{e}^{-i(u+\phi)}d\mathbf{r}\frac{1}{\gamma^2}\int ia\mathrm{e}^{i(u+\phi)}\frac{\partial u}{\partial t}d\mathbf{r}\right\}\\
&= -\int\left(4\sin\theta\ \mathrm{Im}\left\{a\mathrm{e}^{-i(u+\phi)}\frac{1}{\gamma^2}\int a\mathrm{e}^{i(u+\phi)}d\hat{\mathbf{r}}\right\}\right)\frac{\partial u}{\partial t}d\mathbf{r}\\
&= -\int\frac{1}{\eta}\left(\frac{\partial u}{\partial t}\right)^2 d\mathbf{r}, \quad (8)
\end{aligned}$$

where $(\delta V/\delta u)\cdot v = \lim_{\epsilon\to 0}[V(u+\epsilon v) - V(u)]/\epsilon$. Observe that $dV/dt \le 0$, and $dV/dt = 0$ only at equilibria of the dynamics. The feedback system thus evolves to maximize the power in the zero-order Fourier component of the corrected beam. It is clear that $u(\mathbf{r},t) = -\phi(\mathbf{r})$ minimizes $V(u)$, so that phase correction (or phase conjugation) corresponds to energy functional minimization. A standard performance metric for adaptive optic systems is the Strehl ratio, St, which is the normalized zero-order Fourier component intensity,

$$[St(u)](t) = \frac{\left|\frac{1}{\gamma^2}\int a(\mathbf{r})\mathrm{e}^{i[u(\mathbf{r},t)+\phi(\mathbf{r})]}d\mathbf{r}\right|^2}{\left(\frac{1}{\gamma^2}\int a(\mathbf{r})d\mathbf{r}\right)^2}. \quad (9)$$

The Lyapunov functional for the single-pixel Fourier filter is thus proportional to the Strehl ratio [4, 5].

B. *General Fourier phase filter with common phase shift*

If instead of a single Fourier component, multiple Fourier components experience a common phase shift, the (differential) wave-front sensor image (in the absence of any correction) becomes

$$\begin{aligned}
&[f_{common}(\phi)](\mathbf{r})\\
&= \left| a\mathrm{e}^{i\phi} + \left(\mathrm{e}^{i\theta}-1\right)\sum_{\mathbf{p}\in I}\left(\frac{1}{\gamma^2}\int a\mathrm{e}^{i\phi}\mathrm{e}^{-i\frac{2\pi}{\gamma}\mathbf{p}\cdot\mathbf{r}}d\mathbf{r}\right)\mathrm{e}^{i\frac{2\pi}{\gamma}\mathbf{p}\cdot\mathbf{r}}\right|^2\\
&- \left| a\mathrm{e}^{i\phi} + \left(\mathrm{e}^{-i\theta}-1\right)\sum_{\mathbf{p}\in I}\left(\frac{1}{\gamma^2}\int a\mathrm{e}^{i\phi}\mathrm{e}^{-i\frac{2\pi}{\gamma}\mathbf{p}\cdot\mathbf{r}}d\mathbf{r}\right)\mathrm{e}^{i\frac{2\pi}{\gamma}\mathbf{p}\cdot\mathbf{r}}\right|^2\\
&= -4\sin\theta\sum_{\mathbf{p}\in I}\mathrm{Im}\left\{a\mathrm{e}^{-i(\phi-\frac{2\pi}{\gamma}\mathbf{p}\cdot\mathbf{r})}\frac{1}{\gamma^2}\int a\mathrm{e}^{i(\phi-\frac{2\pi}{\gamma}\mathbf{p}\cdot\mathbf{r})}d\mathbf{r}\right\}, \quad (10)
\end{aligned}$$

where I is a finite index set that may or may not contain $\mathbf{0}$.

To state rigorous results for the system of figure 1, we make the following hypotheses:

- periodic boundary conditions on Ω, a square region with sides of length γ;
- initial conditions $u(\mathbf{r},0), Du(\mathbf{r},0), \phi(\mathbf{r}), D\phi(\mathbf{r}) \in L^2(\Omega)$;
- $\eta = \eta(\mathbf{r}) > 0$ and $\frac{1}{\eta} \in L^2(\Omega)$;
- $0 < \theta < \pi$ and $l > 0$;
- I is a finite set;
- $\int[a(\mathbf{r})]^2 d\mathbf{r}$ is bounded; and
- all integrals are understood to be integrals over Ω.

Proposition 1. Weak solutions for equation (4), with f given by equation (10), exist and are unique.

Proof: Straightforward application of methods in [14].

Proposition 2 (from [5]): System (4), with $f(\phi)$ be given by equation (10), is a gradient system with respect to the energy functional

$$\begin{aligned}
V &= \int\frac{l^2}{2}|\nabla u|^2 d\mathbf{r}\\
&- 2\gamma^2\sin\theta\sum_{\mathbf{p}\in I}\left|\frac{1}{\gamma^2}\int a(\mathbf{r})\mathrm{e}^{i(u(\mathbf{r},t)+\phi(\mathbf{r})-\frac{2\pi}{\gamma}\mathbf{p}\cdot\mathbf{r})}d\mathbf{r}\right|^2. \quad (11)
\end{aligned}$$

Specifically, $\partial u/\partial t = -\nabla_u V$ (with respect to the inner product $< g, h >= \int\frac{1}{\eta(\mathbf{r})}g(\mathbf{r})h(\mathbf{r})d\mathbf{r}$ on $L^2(\Omega)$), and

$$\frac{dV}{dt} = -\int\frac{1}{\eta}\left(\frac{\partial u}{\partial t}\right)^2 d\mathbf{r}. \quad (12)$$

Thus, V also serves as a Lyapunov functional for the dynamics; i.e., $dV/dt \le 0$, with $dV/dt = 0$ only at equilibria.

Proof: See [5]. □

The interpretation of the energy functional (11) is analogous to that of equation (7) for the single-pixel Fourier filter. The second term of equation (11) represents the sum of the intensities within the Fourier components of the corrected beam that are phase-shifted by the Fourier filter. The system therefore evolves to maximize the total intensity within the collection of phase-shifted pixels.

C. *General Fourier phase filter with arbitrary phase shifts*

The (differential) wave-front sensor image for arbitrary Fourier component phase shifts is given by

$$\begin{aligned} & f_{arb}(\phi) \\ &= \left| a\mathrm{e}^{i\phi} + \sum_{\mathbf{p}\in I} \left(\mathrm{e}^{i\theta_{\mathbf{p}}} - 1\right) \left(\frac{1}{\gamma^2}\int a\mathrm{e}^{i\phi}\mathrm{e}^{-i\frac{2\pi}{\gamma}\mathbf{p}\cdot\mathbf{r}} d\mathbf{r}\right) \mathrm{e}^{i\frac{2\pi}{\gamma}\mathbf{p}\cdot\mathbf{r}} \right|^2 \\ &- \left| a\mathrm{e}^{i\phi} + \sum_{\mathbf{p}\in I} \left(\mathrm{e}^{-i\theta_{\mathbf{p}}} - 1\right) \left(\frac{1}{\gamma^2}\int a\mathrm{e}^{i\phi}\mathrm{e}^{-i\frac{2\pi}{\gamma}\mathbf{p}\cdot\mathbf{r}} d\mathbf{r}\right) \mathrm{e}^{i\frac{2\pi}{\gamma}\mathbf{p}\cdot\mathbf{r}} \right|^2 \\ &= -4\sum_{\mathbf{p}\in I} \sin\theta_{\mathbf{p}} \mathrm{Im}\left\{ a\mathrm{e}^{-i(\phi - \frac{2\pi}{\gamma}\mathbf{p}\cdot\mathbf{r})} \frac{1}{\gamma^2}\int a\mathrm{e}^{i(\phi-\frac{2\pi}{\gamma}\mathbf{p}\cdot\mathbf{r})} d\mathbf{r} \right\} \\ &\quad + g(\phi), \end{aligned} \tag{13}$$

where the operator $g(\phi)$ is given by

$$\begin{aligned} g(\phi) = & \left| \sum_{\mathbf{p}\in I} \left(\mathrm{e}^{i\theta_{\mathbf{p}}} - 1\right) \left(\frac{1}{\gamma^2}\int a\mathrm{e}^{i\phi}\mathrm{e}^{-i\frac{2\pi}{\gamma}\mathbf{p}\cdot\mathbf{r}} d\mathbf{r}\right) \mathrm{e}^{i\frac{2\pi}{\gamma}\mathbf{p}\cdot\mathbf{r}} \right|^2 \\ & - \left| \sum_{\mathbf{p}\in I} \left(\mathrm{e}^{-i\theta_{\mathbf{p}}} - 1\right) \left(\frac{1}{\gamma^2}\int a\mathrm{e}^{i\phi}\mathrm{e}^{-i\frac{2\pi}{\gamma}\mathbf{p}\cdot\mathbf{r}} d\mathbf{r}\right) \mathrm{e}^{i\frac{2\pi}{\gamma}\mathbf{p}\cdot\mathbf{r}} \right|^2 . \end{aligned} \tag{14}$$

By taking $g(\phi) \equiv 0$ in equation (13), we obtain a nonlinear approximation to the wave-front sensor image. Simulation and experimental work suggest that this nonlinear approximation adequately captures the system's qualitative behavior [4].

Proposition 3: Under the same hypotheses as **Proposition 2**, system (4), with $f = f_{arb} - g$, is a gradient system with respect to the energy functional

$$\begin{aligned} V = & \int \frac{l^2}{2} |\nabla u|^2 d\mathbf{r} \\ & - 2\gamma^2 \sum_{\mathbf{p}\in I} \sin\theta_{\mathbf{p}} \left| \frac{1}{\gamma^2} \int a(\mathbf{r}) \mathrm{e}^{i(u(\mathbf{r},t)+\phi(\mathbf{r})-\frac{2\pi}{\gamma}\mathbf{p}\cdot\mathbf{r})} d\mathbf{r} \right|^2 . \end{aligned} \tag{15}$$

Also, V serves as a Lyapunov functional for the dynamics.

Proof: Analogous to the proof of **Proposition 2**. □

IV. Practical implementation issues

For a single-pixel Fourier filter, image contrast suffers when the beam is highly aberrated, a problem that can be overcome by using a multi-pixel Fourier filter. The theoretical work presented here and in [5] indicates that even for a multi-pixel Fourier filter, a gradient dynamics property can hold, so that phase-shifting multiple Fourier components need not upset the convergence behavior of the system of figure 1.

A. *Thresholding Fourier filter operator*

An example of a Fourier filter operator that would give rise to Fourier filters of the type described by equation (10) is to compare the Fourier-domain intensity, on a pixel-by-pixel basis, to a threshold, and phase-shift the pixel by θ if that threshold is exceeded. This type of wave-front sensor has been studied numerically and found to yield a higher-contrast image than a single-pixel Fourier filter for highly aberrated beams [3]. However, when incorporated into the feedback system of figure 1, this thresholding wave-front sensor fails to evolve into a single-pixel sensor as wave-front correction proceeds. Instead, the system generally approaches an equilibrium with the corrected beam intensity distributed among a number of Fourier components.

B. *Proportional Fourier filter operator*

A simple Fourier filter operator which is observed to produce wave-front correction is the proportional Fourier filter operator, in which Fourier components are phase-shifted in proportion to their power [3]. Since different Fourier components experience different phase shifts, for a given Fourier intensity distribution, the wave-front sensor image can be described by equation (13).

Comparing equations (11) and (15) suggests why the system with a proportional Fourier filter operator outperforms the system with the thresholding operator. For the (approximate) proportional Fourier filter operator, the Lyapunov functional is minimized by concentrating all of the intensity in the Fourier component (or components) *with the greatest phase shift* (provided $\theta_{\mathbf{p}} \leq \pi/2, \ \forall \mathbf{p}$). However, for the thresholding Fourier filter operator, there is no preference (in terms of Lyapunov functional minimization) for any particular distribution of intensity among the Fourier components phase-shifted by θ.

Note that **Propositions 2 and 3** apply to systems with fixed Fourier filters, even though in the system of figure 1, the Fourier filter evolves in time as phase correction proceeds. We are inferring how the system with an evolving Fourier filter will behave from the analysis for fixed Fourier filters.

V. Wave-front estimator analysis

The analysis of Section III demonstrates that high-resolution wave-front control is feasible, in the sense that there exists a parallel, distributed feedback control approach which (with some simplifications and approximations) tends to converge to an equilibrium representing wave-front correction. Furthmore, the analysis is nonlinear and global, but is deterministic. To properly design and assess the performance of an adaptive optic system for atmospheric turbulence compensation, it is imperative to consider the statistical nature of atmospheric turbulence and photodetector noise.

General problem formulation: Subject to constraints of realizability, how can atmospheric turbulence compensation be performed optimally, given stochastic models for the wave-front distortion and photodetector noise?

Instead of this general problem, we consider the following.

Weaker problem formulation: Subject to constraints of realizability, how can atmospheric turbulence compensation be performed nearly optimally when the residual distortion is small, and adequately when the residual distortion is large,

given simplified stochastic models for the wave-front distortion and photodetector noise?

To investigate this weaker formulation, we discretize both the time and spatial variables, and consider the system of figure 1 to be a nonlinear estimator: based on noisy, nonlinear measurements of the corrected beam wave front, the system attempts to estimate the (conjugate of the) input beam wave front.

A. *Modeling wave-front distortion and photon noise*

Very detailed statistical models of atmospheric turbulence and photon noise can be found in the literature, and have been used to study and design adaptive optic systems [13]. Statistical models for atmospheric turbulence generally assume particular forms for the spatial power spectra, with origins in the study of thermal energy transfer and fluid motion across various length scales. Motion of the turbulent structures produces the temporal dependence of the wave-front distortion.

A standard approach for modeling photon noise is the semi-classical model [13]. Electromagnetic field theory is used to describe the system up to the plane where the intensity measurement is made. The intensity measurement is then taken to be a Poisson process with its rate function determined by the classical electromagnetic field irradiance. (Integrating the rate function over the area of a single photodetector gives the average number of photons incident on the detector per unit time.) The electromagnetic field irradiance depends on both the deterministic optical system (i.e., the operator f of Section III), and the random atmospheric turbulence.

Rather than use the detailed, realistic models for turbulence and photon noise, we instead use simple models with parameters derived from the more detailed models. These are the simplifying assumptions we make:

- The phase-correcting SLM spatial discretization is matched to the smallest feature size present in the distortion, so that the wave front can be approximated as piecewise constant (i.e., constant over the area of a phase-correcting SLM pixel). The Fried parameter, dependent on wavelength and the strength of turbulence, is proportional to this smallest feature size [13].
- For each phase-correcting SLM pixel, the change in input beam wave front from one time step to the next is independent and normally distributed.
- The input beam intensity distribution is quasi-static, so that for purposes of the analysis it is taken to be constant, although it may vary spatially.
- The Poisson distribution for photon noise is approximated as a Gaussian distribution with the same mean and variance (a reasonable approximation as long as the intensity is not too low), so that the photon noise process is modeled as independent and normally distributed.

B. *Nonlinear estimator*

We let k denote the discrete time variable, and we let $\mathbf{s}$, a two-dimensional vector of integers, denote the discrete transverse coordinates. For the wave-front estimation problem we use a discrete Fourier transform:

$$A_{\mathbf{s}} = \sum_{\mathbf{p}} \mathrm{a}_{\mathbf{p}} \mathrm{e}^{i\frac{2\pi}{n}\mathbf{p}\cdot\mathbf{s}},$$

$$\mathrm{a}_{\mathbf{p}} = \frac{1}{n^2}\sum_{\mathbf{s}} A_{\mathbf{s}} \mathrm{e}^{-i\frac{2\pi}{n}\mathbf{p}\cdot\mathbf{s}}, \tag{16}$$

where the $\mathrm{a}_{\mathbf{p}}$ now represent discrete Fourier transform coefficients. The total number of grid points (in both the spatial and Fourier domains) is n^2.

The state of the distortion (specifically, the effect of the atmospheric turbulence on input beam phase) is denoted $\phi_{\mathbf{s}}(k)$. We assume that the update equation for the atmosphere is

$$\phi_{\mathbf{s}}(k+1) = \phi_{\mathbf{s}}(k) + w_{\mathbf{s}}(k), \tag{17}$$

where the $w_{\mathbf{s}}(k)$ are independent and normally distributed, with (scalar) covariances $q_{\mathbf{s}}(k)$ (which are reasonable to assume are equal for all $\mathbf{s}$).

The estimate of the state of the distortion at time k (given information up to time $k-1$) is denoted $\hat{\phi}_{\mathbf{s}}(k|k-1)$. The error signal,

$$\varepsilon_{\mathbf{s}}(k) = \phi_{\mathbf{s}}(k) - \hat{\phi}_{\mathbf{s}}(k|k-1), \tag{18}$$

is produced by the phase-correcting SLM, and is what we would like the wave-front control system to minimize (in an appropriately weighted mean-square sense). We let $\boldsymbol{\varepsilon}(k)$ denote the matrix $\{\varepsilon_{\mathbf{s}}(k)\}$. In the absense of measurement noise, the image measured by, e.g., the single-pixel differential Zernike wave-front sensor can then be expressed as

$$[f(\boldsymbol{\varepsilon})]_{\mathbf{s}}(k) = -4\sin\theta\ \mathrm{Im}\left\{ a_{\mathbf{s}} \mathrm{e}^{-i\varepsilon_{\mathbf{s}}(k)} \frac{1}{n^2} \sum_{\bar{\mathbf{s}}} a_{\bar{\mathbf{s}}} \mathrm{e}^{i\varepsilon_{\bar{\mathbf{s}}}(k)} \right\}. \tag{19}$$

The measured image including photon noise is then $[f(\boldsymbol{\varepsilon})]_{\mathbf{s}}(k) + v_{\mathbf{s}}(k)$, where we assume the $v_{\mathbf{s}}(k)$ are independent and normally distributed, with (scalar) covariances $r_{\mathbf{s}}(k)$.

A natural update equation for the estimator is

$$\hat{\phi}_{\mathbf{s}}(k+1|k) = \hat{\phi}_{\mathbf{s}}(k|k-1) + c_{\mathbf{s}}(k)\left([f(\boldsymbol{\varepsilon})]_{\mathbf{s}}(k) + v_{\mathbf{s}}(k)\right), \tag{20}$$

where $\{c_{\mathbf{s}}\}$ is a gain matrix (replacing the gain function $\eta(\mathbf{r},t)$ of Section III). Equation (20) is a discrete-time (and spatially discretized) version of the deterministic gradient flow (4), with $l=0$, and with additional noise terms. The evolution equation for the error is

$$\varepsilon_{\mathbf{s}}(k+1) = \varepsilon_{\mathbf{s}}(k) - c_{\mathbf{s}}(k)\left([f(\varepsilon)]_{\mathbf{s}}(k) + v_{\mathbf{s}}(k)\right) + w_{\mathbf{s}}(k). \tag{21}$$

We thus have a nonlinear update equation for the estimation error, involving both process and measurement noise. We would like to analyze the stability and convergence properties of equation (21).

C. *Relationship between Strehl ratio and error covariance*

A natural performance metric for wave-front estimation is the weighted sample error covariance

$$\varphi(\boldsymbol{\varepsilon}) = \frac{\frac{1}{n^2}\sum_{\mathbf{s}} a_{\mathbf{s}}(\varepsilon_{\mathbf{s}} - \bar{\varepsilon})^2}{\frac{1}{n^2}\sum_{\mathbf{s}} a_{\mathbf{s}}}, \tag{22}$$

where

$$\bar{\varepsilon} = \frac{\frac{1}{n^2}\sum_{\mathbf{s}} a_{\mathbf{s}}\varepsilon_{\mathbf{s}}}{\frac{1}{n^2}\sum_{\mathbf{s}} a_{\mathbf{s}}}. \tag{23}$$

The relationship between the Strehl ratio and the wave-front error covariance is well-known in the optics literature [13]. For concreteness, we outline a derivation.

The zero-order Fourier component intensity is

$$i_0(\boldsymbol{\varepsilon}) = (\mathrm{a_0})^2 = \left| \frac{1}{n^2} \sum_{\mathbf{s}} a_{\mathbf{s}} \mathrm{e}^{i\varepsilon_{\mathbf{s}}} \right|^2 . \tag{24}$$

The Strehl ratio, $St(\boldsymbol{\varepsilon}) = i_0(\boldsymbol{\varepsilon})/i_0(\bar{\boldsymbol{\varepsilon}})$, can be shown to satisfy

$$St(\boldsymbol{\varepsilon}) = 1 - \varphi(\boldsymbol{\varepsilon}) + \text{h.o.t.} \tag{25}$$

To see this relationship between Strehl ratio and error covariance, simply take the Taylor series expansion of $i_0(\boldsymbol{\varepsilon})$ around $\bar{\boldsymbol{\varepsilon}}$,

$$i_0(\boldsymbol{\varepsilon}) = i_0(\bar{\boldsymbol{\varepsilon}}) + \frac{\partial i_0}{\partial \boldsymbol{\varepsilon}}\bigg|_{\bar{\boldsymbol{\varepsilon}}} \cdot (\boldsymbol{\varepsilon} - \bar{\boldsymbol{\varepsilon}}) + \frac{1}{2}\frac{\partial}{\partial \boldsymbol{\varepsilon}}\left(\frac{\partial i_0}{\partial \boldsymbol{\varepsilon}}\right)\bigg|_{\bar{\boldsymbol{\varepsilon}}} \cdot [(\boldsymbol{\varepsilon} - \bar{\boldsymbol{\varepsilon}}), (\boldsymbol{\varepsilon} - \bar{\boldsymbol{\varepsilon}})] + \cdots , \tag{26}$$

where $\bar{\boldsymbol{\varepsilon}}$ denotes the $n \times n$ matrix whose elements are all $\bar{\varepsilon}$. Computing the partial derivatives in equation (26) gives

$$i_0(\boldsymbol{\varepsilon}) = i_0(\bar{\boldsymbol{\varepsilon}})\,(1 - \varphi(\boldsymbol{\varepsilon})) + \text{h.o.t.} \tag{27}$$

There is thus a straightforward relationship between Strehl ratio maximization for the deterministic wave-front control problem and error covariance minimization for the wave-front estimation problem. The Strehl ratio can be measured using the Fourier-domain imager in figure 3, which raises the possibility of adapting the gain matrix on-line.

D. *Implications for system design*

Our general strategy for system design is then to start with the basic architecture of figure 1, and make good choices for the Fourier filter operator and the gain matrix. We have seen from the deterministic analysis that the proportional Fourier filter operator (with the peak phase shift constrained to be at most $\pi/2$) has favorable properties. For the stochastic system, it is critical that the Fourier filter provide a filtered image with good signal-to-noise ratio (i.e., good constrast), so that the system can start compensating phase distortion even when the initial distortion is severe.

The deterministic analysis of Section III places no constraints on the gain function (other than a sign condition and the $L^2(\Omega)$ property of $1/\eta$). However, in the discrete-time setting, the dynamical equation (4) is replaced by a forward-Euler method, and it is evident that there is an upper limit on each element of the gain matrix. For linear estimation problems, the gains start out large, and decrease as the estimate is refined. A similar behavior is expected for the nonlinear estimator described above. Our strategy is then to make sure the gain matrix elements stay bounded appropriately (to ensure stability of the nonlinear system) when the estimation error is large, and to reduce the gain matrix (e.g., using a common scale factor) as the estimation error decreases. In the small-estimation-error regime, a linear approximation to the nonlinear estimator may be useful. By scaling the gain matrix based on the measured Strehl ratio, the system can transition naturally on its own from the nonlinear, large-distortion regime to the linear, small-distortion regime.

VI. Summary and conclusions

Large arrays of sensors and actuators are becoming feasible to build. However, using such arrays for feedback control of physical fields depends critically on our ability to devise control schemes for such systems. Optics is a natural context in which to investigate such control schemes, because there has been considerable experimental work in adaptive optics to draw upon, and because optics can be useful for measurement in other engineering contexts, as well.

However, in considering optical wave-front measurement and control, nonlinearity enters in an intrinsic way. We need to be able to deal with the nonlinearity, as well as with the constraints arising from having to use a parallel, distributed control scheme rather than a centralized control law. The strategy of identifying a nonlinear approximation to the dynamics which captures its essential features even far from equilibrium can be simpler to carry out, and more revealing, than a linearized analysis about the equilibrium. Furthermore, the results can be used to guide design.

Acknowledgments

The authors would like to thank Mikhail Vorontsov of the Army Research Laboratory, Adelphi, MD; Ralph Etienne-Cummings of Johns Hopkins University, Baltimore, MD; and Steve Serati and Teresa Ewing of Boulder Nonlinear Systems, Inc., Lafayette, CO, for valuable discussions.

References

[1] S. A. Serati, G. D. Sharp, R. A. Serati, D. J. McKnight, and J. E. Stockley, "128 x 128 analog liquid crystal spatial light modulator," Optical Pattern Recognition VI, *Proc. SPIE*, **2490**, 378-387, 1995.

[2] M. Horenstein, T.G. Bifano, S. Pappas, J. Perreault, and R. Krishnamoorthy-Mali, "Real Time Optical Correction Using Electrostatically Actuated MEMS Devices." *Journal of Electrostatics,* **46**, 91-101, 1999.

[3] M.A. Vorontsov, E.W. Justh, and L.A. Beresnev, "Adaptive Optics with Advanced Phase-Contrast Techniques: Part I. High-Resolution Wavefront Sensing," *Journal of the Optical Society of America A*, to appear, 2001.

[4] E.W. Justh, M.A. Vorontsov, G.W. Carhart, L.A. Beresnev, and P.S. Krishnaprasad, "Adaptive Optics with Advanced Phase-Contrast Techniques: Part II. High-Resolution Wavefront Control," *Journal of the Optical Society of America A*, to appear, 2001.

[5] E.W. Justh, P.S. Krishnaprasad, and M.A. Vorontsov, "Nonlinear Analysis of a High-Resolution Optical Wavefront Control System," *Proc. 39th IEEE Conf. Decision and Control*, 3301-3306, IEEE, New York, 2000.

[6] F. Zernike, "How I Discovered Phase Contrast," *Science*, **121**, 345-349, 1955.

[7] J.W. Goodman, *Introduction to Fourier Optics*, McGraw-Hill, New York, 1996.

[8] *SPIE Proc., Phase Contrast and Differential Interference Contrast Imaging Techniques and Applications,* **1846**, 1994.

[9] V.Yu. Ivanov, V.P. Sivokon, and M.A. Vorontsov, "Phase retrieval from a set of intensity measurements: theory and experiment," *J. Opt. Soc. Am. A*, **9**(9), 1515-1524, 1992.

[10] J. Glückstad, "Adaptive array illumination and structured light generated by spatial zero-order self-phase modulation in a Kerr medium," *Optics Communications*, **120**, 194-203, 1995.

[11] A. Seward, F. Lacombe, and M. K. Giles, "Focal plane masks in adaptive optics systems," Adaptive Optics Systems and Technology, *Proc. SPIE*, **3762**, 283-293, 1999.

[12] V. Gruev and R. Etienne-Cummings, "A programmable spatiotemporal image processor chip," *Proc. IEEE International Syposium on Circuits and Systems,* **IV**, 325-328, 2000.

[13] M.C. Roggeman and B. Welsh, *Imaging through turbulence*, CRC Press, Boca Raton, 1996.

[14] Lawrence Craig Evans. *Partial Differential Equations.* American Mathematical Society, Providence, 1998.